Thermal and microstructure study of the chip formation during turning of Ti64 β lamellar titanium Structure

Vincent Wagner, Floran Barelli, Gilles Dessein, Raynald Laheurte, Phillipe Darnis, Olivier Cahuc, Michel Mousseigne

Vincent Wagner[1]
Laboratoire Génie de Production (LGP)
INP-ENIT,
Université de Toulouse,
Tarbes 65000, France
e-mail: vincent.wagner@enit.fr

Floran Barelli
HAM France Andreas Maier,
Chemin de la Forêt,
Peillonnex 74250, France

Gilles Dessein
Laboratoire Génie de Production (LGP)
INP-ENIT,
Université de Toulouse,
Tarbes 65000, France

Raynald Laheurte
Université de Bordeaux,
CNRS, I2M Bordeaux,
351 cours de la Libération,
Talence F-33400, France

Phillipe Darnis
Université de Bordeaux,
CNRS, I2M Bordeaux,
351 cours de la Libération,
Talence F-33400, France

Olivier Cahuc
Université de Bordeaux,
CNRS, I2M Bordeaux,
351 cours de la Libération,
Talence F-33400, France

Michel Mousseigne
Institut Clément Ader (ICA),
CNRS, UPS, INSA, ISAE-SUPAERO, Mines-Albi,
Université de Toulouse,
3 rue Caroline Aigle,
Toulouse 31400, France

Thermal and Microstructure Study of the Chip Formation During Turning of Ti64 β Lamellar Titanium Structure

In recent years, many titanium alloys have emerged, each of them associated with a range of different heat treatments. Thus, several microstructures have been studied to varying degrees. For example, the Ti64 titanium alloy, mostly known for its $\alpha + \beta$ structure, can display a different state: the structure, inducing nonstandard mechanical behavior. This work presents chip formation in this specific microstructure where a strong heterogeneity is observed and where the shear band formation is a function of the relationship between the shear direction and the microstructure orientation. From these reasons, major differences are found in the chip morphology, within the same cutting condition, in comparison to the bimodal structure where a single chip morphology is obtained for each cutting condition. A section of this paper is devoted to the presentation of the β microstructure where different configurations can be seen within the same chip. Next, the influence of cutting conditions on the chip formation is studied. To highlight the specific chip formation process, a temperature model has been developed and combined with cutting force analysis to understand clearly the specificity of the chip formation for this structure. Finally, the discussion explains the different chip formation scenarios according to the workpiece microstructure to be cut. [DOI: 10.1115/1.4038597]

1 Introduction

For many years, the machining of titanium alloys has been a very significant issue in the aeronautical industry. This difficulty is related to the low machinability of titanium alloys but also to their diversity. In recent years, many alloys of titanium (Ti-64, Ti-1023, Ti-5553, Ti-17, etc.) have emerged. The low machinability can be explained in five points:

- The low thermal conductivity which can increase the temperature at the tool chip interface.
- The strong chemical affinity with the cutting tool materials can generate chip welded, and this is increased by the high temperature involved by the cutting process.
- The titanium alloy's mechanical properties. For example, the elastic modulus is lower than that of steel. Consequently, some chatter and fluctuations can occur during the process.
- The contact length between the chip and the rake face is short and causes an increase in cutting temperatures, stresses, and forces.

- Finally, the surface integrity is sensitive to the cutting speed and can be affected at high cutting speeds. To limit these effects, the cutting conditions are usually chosen small.

Moreover, the number of titanium alloys has increased drastically and their structure may be different and induce various specific chip formations. Over a number of years, certain works have studied chip formations in different alloys. One of them concerns the Ti64 $\alpha + \beta$ carried out by Komanduri and Von Turkovich [1] and Vyas and Shaw [2]. Since then, different studies have been performed on the same alloy by Barry et al. [3] and Nouari and Makich [4] and on the Ti1023 (β structure) by Wagner and Duc [5], the Ti5553 (a near β metastable) [6–8], and the Ti17 [9]. However, the majority of these papers concern the machining of bimodal structures where α nodules occur in the β matrix. Different theories have been proposed about chip formation, and especially the shear bands formation in the primary zone. Shaw and Vyas [10] considered that these bands are initiated at the free surface of the chip (upper side/uncut chip). The shear band is then a crack which is directed to the cutting tool edge. Some other theories go the opposite way. Indeed, based on the assessments of Recht [11] and according to the authors of Refs. [1], [12], and [13], the shear band is created near to the cutting edge and propagates toward the free surface of the chip. The most important

point is the nature of the primary zone which is defined as a shearing unlike Shaw and Vyas [10] who consider the primary zone as being a crack. Guosheng and Zhanqiang [14] explained that the chip formation is generated by the cutting edge where a significant compression occurs. Pottier et al. [15] and more recently Harzallah et al. [16] proposed a new theory of chip formation. This chip formation analysis is defined by numerical models and video acquisitions of the chip formation. This is based on three steps: the germination, the growth, and the extraction. During the first step, a strong hydrostatic compressive loading induced by the tool tip generates high deformations within the material. These deformations occur along the primary shear plane and out of this plane. This step is complete when a microcrack occurs. The growth step corresponds to the crack's evolution in the primary shear plane direction. This step is characterized by a large thermal dissipation. This occurs with an important increase of temperature and strain rate with a strong decrease of Von Mises stress. These phenomena expose the thermal softening which occurs in the primary shear plane. The final step begins when the crack formation is complete. Consequently, the segment slide on the rake face. The temperature is further stabilized, and the residual stress in the chip is very important. Sutter and List [17] exposed a new analysis of creation and modification of segments for very high cutting speed. This new purpose is based on photographs taken during machining. The chip formation follows a repetitive and cyclic phase which occurs once the preceding segment is removed. To complete the chip formation, understanding lot of works and numerical model has been developed for titanium alloys [18] or more recently in introducing the sensitivity of the microstructure [19]. However, all these works concern an identical structure. Chips are always saw-tooth where the α nodules are sheared in the primary zone (Fig. 1) according to one direction (shear angle). The distance between two primary zones is dependent on the cutting conditions (cutting speed and feed). In the secondary shear zone, the α nodules are sheared in the same direction as the chip velocity. This stable chip formation occurs despite the heterogeneity of the structure as exposed by Arrazola et al. [7] for the chip formation and Nguyen et al. [20] for the flank wear.

Based on these points, the purpose of this paper is to provide an experimental analysis of chip formation for a different microstructure of the Ti64 alloy: Ti64 β. This work comprises several sections. The first one outlines the experimental setup where the structure is presented. Following this presentation, the chip formation of the Ti64 β structure is analyzed. To complete the analysis of the chip formation, a specific model of temperature has been developed. This section ends with a detailed analysis of chip formation and identification of different scenarios which explain this chip formation. To finish, a conclusion sums up all the results.

2 Experimental Setup

The composition of Ti64 is 6% aluminum and 4% of vanadium, the rest being titanium. The recrystallization process comprises different steps and generates, as the additional elements, the Ti64 microstructure.

The Ti64 β structure is different (Fig. 2). Generally, titanium is composed of two allotropic phases. The first is the α phase (hexagonal close packed), and the second is the β phase (body-centered cubic). When the titanium is natural, the α phase is stable when the temperature is lower than $882\,^{\circ}\mathrm{C}$, contrary to the β phase which is stable when the temperature is higher than $882\,^{\circ}\mathrm{C}$ but lower than the fusion temperature. The β transus temperature (T_β), at the limit between α and $\alpha + \beta$ domain, is a function of additional elements. Concerning the Ti64, betagene elements such as vanadium stabilize the transus β temperature for low temperatures. Consequently, this alloy can be two-phase $(\alpha + \beta)$ for low temperatures, unlike alphagene elements such as aluminum, which increases the transus temperature [21].

The Ti64 microstructure is a function of the different steps of the recrystallization process [22,23]. Figure 2 shows the heat treatment and the microstructure analysis. The aim of this section provides a description of the heat treatment and the different phases of the titanium alloys. The heat treatment comprises four steps. The first is a homogenization of the structure. Next is the forging in the $\alpha + \beta$ domain. A solution heat treatment which begins in the β domain is then carried out with a long cooling period. Finally, an aging is performed at a temperature lower than the transus β temperature.

If the process is carried out in the β domain and followed by an energetic hardening, the β phase will undergo a martensitic transformation creating a needle structure. When the cooling rate decreases, the needle diameters increase until the needles become wide lamellae. The structure is also lamellar as for this study.
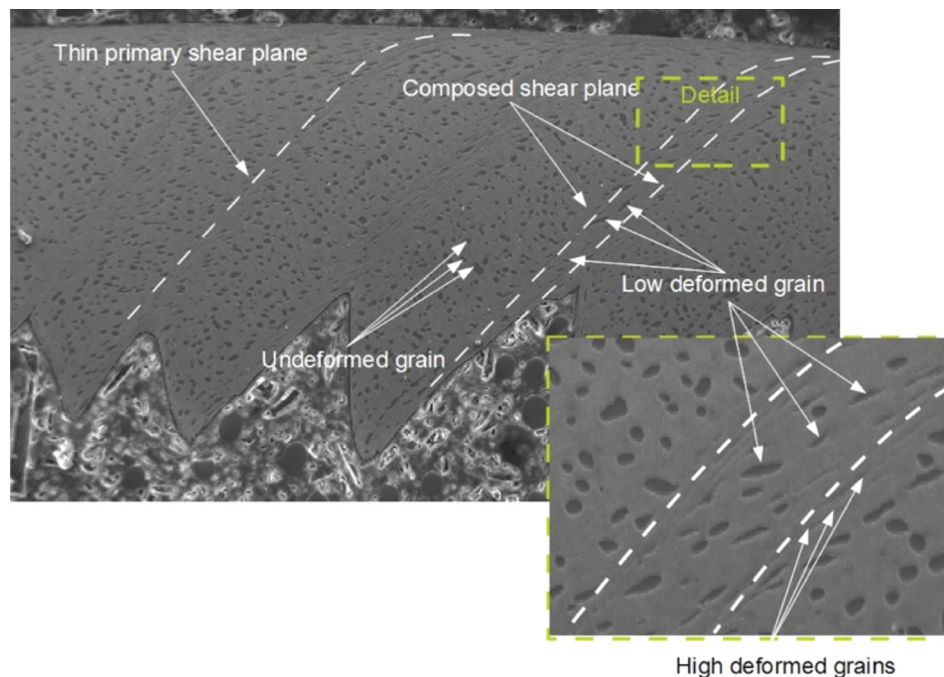

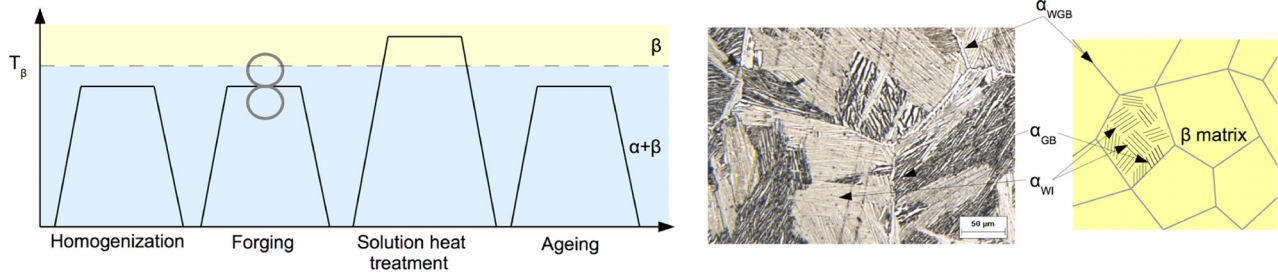Fig. 1 Chip formation during Ti5553 turning [8]

Fig. 2 Heat treatment of titanium alloy (*a*) and Ti64 *β* microstructure (*b*)

When the recrystallization process is carried out in the $\alpha + \beta$ domain, the primary α slates are generated and are amalgamated to β grains. The additional elements migrate into specific phases: the primary α phase for aluminum and the β phase for vanadium. It is during the cooling that the secondary α lamellae are trapped into β grains [21], thus resulting in a two-phase structure as well.

In opposition to the classical microstructure, the Ti64 *β* structure is totally lamellar (Fig. 2), α phases transforming to an acicular α′ structure in the *β* matrix [22]. It is possible to observe the phase α_{BG} near to the grain joint in Fig. 2. It occurs as a continuous line around the old β grain. Concerning the phase α_{WBG}, it germinates from the seal of the grain to the center and occurs in the form of slate. Finally, the α_{WI} phase germinates inside the old β grain. All these phases are surrounded by the β matrix.

Mechanical properties for the Ti64 $\alpha + \beta$ are $R_m = 1100$ MPa and $VHN = 349$ HV and concerning the Ti64 *β* $R_m = 1050$ MPa and $VHN = 338$ HV.

All tests were carried out on a Somab Genimab 900 CNC lathe. The tool inserts are CCMX 120408 with TiN PVD coating. The rake angle is 20 deg, the clearance angle is 7 deg, and the inserts have a simple chamfer edge preparation of 0.02 mm. This geometry was selected among the tools proposed for titanium machining. A tubular workpiece of 3 mm in width was chosen which allows us to limit the speed variation on the cutting edge. All tests were performed with dry machining. For conditions to be in industry, the cutting conditions were defined according to the French Tool Material Pair standard [24] and they are summed up in Table 1. All tests and all measures were performed three times and the standard deviation is often lower at 5% of the range.

The microstructures were studied from observations by optical microscopy and scanning electron microscopy (FEG-SEM JEOL 7000F).

3 Chip Formation

For this structure, the chip formation and especially the shear band formation is different. The formation is not only due to shearing generated between the tool edge and the free surface of the chip. Indeed, several phenomena can be observed due to the alloy structure which is composed of lamellar colonies $\alpha + \beta$ with different orientations. The observations show that shear band formation is a function of colony orientations. Figure 3 shows that various shear phenomena observed in the same chip which induces chip geometry evolve.

This first section is devoted to observe the different phenomena that occur in the chip inside the β structure. Indeed, the analysis of

Table 1 Cutting conditions for each test

Test	V_c (m/min)	t_u (mm)
1	40	0.07
2	50	0.07
3	65	0.07
4	65	0.1
5	65	0.13
6	65	0.16
7	65	0.19

the microstructure shows some areas where the old structure and the old β grain occur. The work reported in this section corresponds to the assessment made of the analysis of all the lengths of all the chips generated. Indeed, it is clear that in the β structure, only four configurations favoring or limiting the formation of the primary shear band have been observed.

3.1 First Configuration. Whatever the cutting conditions, some cracks may be generated near a primary shear band (Fig. 4). Two causes are further identified. The first is similar to the classical structure ($\alpha + \beta$). The crack is also due to a very high shear strain which occurs in the material [1]. The second cause is specific to this structure. It is due to an accumulation of plastic strain at the interface between two lamellar colonies with a strong misorientation (colony 1 versus colony 2 and colony 3 versus colony 4 on Fig. 4). This strain accumulation is explained by the difficulty in providing dislocations between two misoriented colonies. Indeed, the Burger vector difference of orientation is too great between the two colonies [21] and the plastic strains are stacked on colony bounds. When the adiabatic shear band is formed, strains are then generated collinearly to the shear angle. As was described, the direction of the shear band can be variable. When the adiabatic shear bands are formed and tries to meet the free surface of the chip, it can meet two completely disoriented colonies. Dislocations then accumulate at the interface and a crack is created owing to stress concentration.

3.2 Second Configuration. The adiabatic shear bands are preferably generated in lamellar colonies transverse to the shear band direction. As seen in Fig. 5, the primary bands are generated only in the transversal colony. Indeed, in the highlighted zone where the lamella orientation is different, no primary shear bands are generated. This point can affect the frequency of shear band formation. As seen in Fig. 3, the distance of primary shear bands can be different according to the colony orientation. Although the interface $\alpha + \beta$ can spread the dislocations, a stress gradient exists between the different *β* lamellae with the highest value located at the interface. So, the deformation required to shear the interface is greater than that required to shear the α lamellae located at the interfaces, and thus shearing occurs through shear bands. The shear bands' thickness appears to be a function of the colonies' orientation.

3.3 Third Configuration. The colonies oriented as the shear band formation (primary zone) can be sheared transversally. This shearing is imposed by the motion between the surrounding colonies. Two shearing directions are observed (Fig. 6). The first is collinear to the upper grain boundary (black line). As seen in Fig. 6, this phenomenon is limited to a part of the grain. Indeed, only a section of the grain has the transversal shearing. The second direction is collinear to the interface between the observed colony and the secondary shear zone (blue line).

3.4 Fourth Configuration. The last configuration shows that continuous shearing can occur near the free edge of the chip (Fig. 7). The shearing follows the motion imposed at the chip extremity (red arrow) and at the interface of the nearest colony

(blue arrow). Consequently, and due to this effect, some adiabatic shear bands occur at the free edge of the chip.

4 Cutting Condition Effects

4.1 Cutting Forces and Cutting Temperatures. To understand the effect of the cutting conditions (cutting speed and feed) on the chip formation, some additional tests were conducted. The conditions chosen were the classical ones used for titanium machining. The chip formation comparison is performed by the analysis of different points: the cutting forces F_c and F_r, respectively, the component according to cutting speed direction and feed direction, and finally, the temperature in primary sheared zone (T_1).
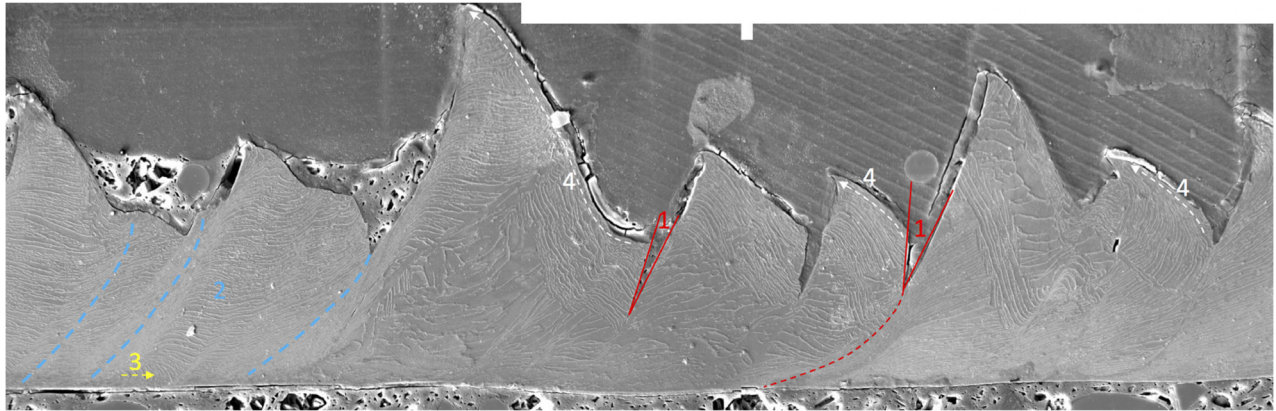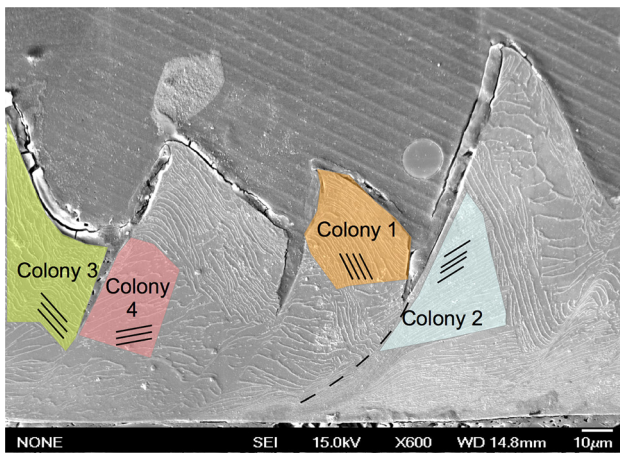

Fig. 3   Chip morphology for Ti64 β

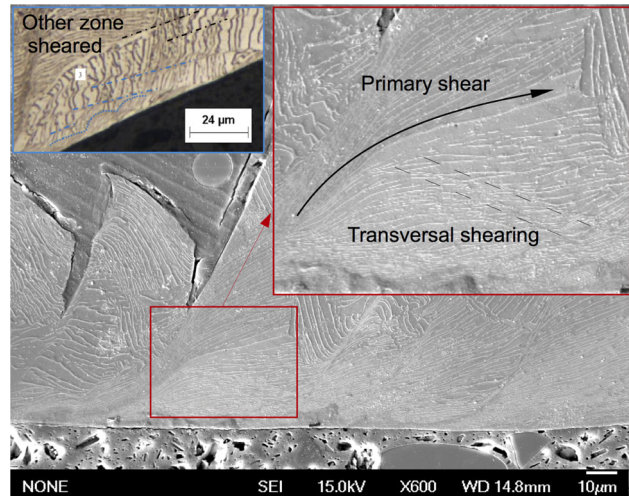**Fig. 4   First configuration**

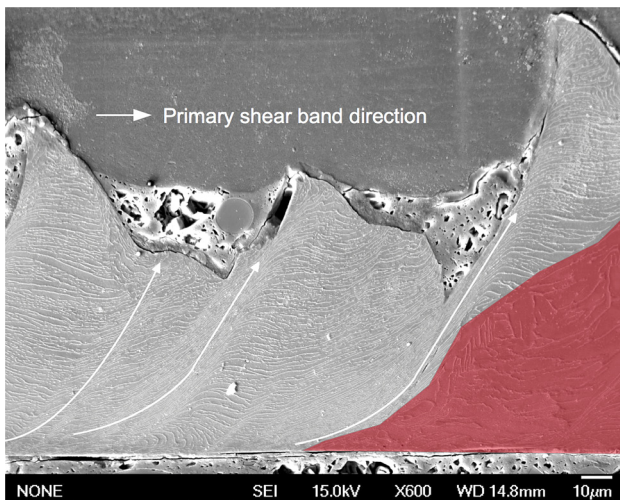**Fig. 6   Third configuration**

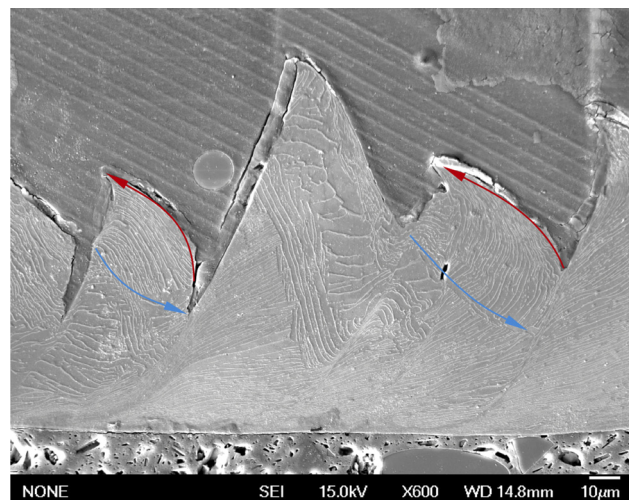**Fig. 5   Second configuration**

Fig. 7   Fourth configuration

Concerning the cutting forces, their monitoring serves to characterize the alloy behavior (Fig. 8). Due to the orthogonal configuration, the component collinear to the cutting edge is not existent. The two components (F_c and F_r) are constant when the cutting speed increases. This is mainly due to the low effect of the temperature on the mechanical properties of titanium alloy. The high level of the thermal softening compared to the hardening is never reached despite high heat generated during the chip formation. Contrary to the cutting speed, the increase of feed generates some highest cutting forces. This conclusion is particularly true of the F_c component which increases linearly with the feed.

However, and as defined previously, the specific chip formation limits the use of classical models such as Oxley's one to define the cutting temperatures. Indeed, the nonconstant volume of sheared material combined with the noncyclic phenomena restricts its use. To define the cutting temperatures, a specific method has been developed. It is based on the power distribution which occurs during chip formation [25]. During this process, the power supplied by the tool (W_{ext}) is mostly consumed in two zones: the primary shear zone (W_{Z1}) and the secondary shear zone (W_{Z2}). For this study, the power generated between the flank face and the workpiece surface (third zone) is not considered. The power consumption of the two zones is governed by the predominant phenomena observed in each zone, namely, plasticity for the primary zone and friction for the second zone

$$W_{ext} = W_{Z1} + W_{Z2} \tag{1}$$

The energy brought inside the workpiece material is always

$$W'_{ext} = F_c V_c \tag{2}$$

where W'_{ext} is the external power in (W), V_c is the cutting speed in (m/s), and F_c is the cutting forces (N).

To define the power consumed, one of the possibilities is to use the heat equation where

$$\rho C_p \frac{\partial T}{\partial t} - \nabla(K \nabla T) = \omega'_{heat} \tag{3}$$

in applying the hypothesis of adiabaticity mostly used to explain chip formation [1], it is also possible to define locally the following equation:

$$\rho C_p \frac{\partial T(x,t)}{\partial t} = \omega'_{heat} \tag{4}$$

where ρ is the density (kg/m^3), C_p is the specific heat (J/kg K), and ω'_{heat} is the power dissipated in heat per volume (W/m^3).

Based on the main phenomena of each zone, it is possible to define the power consumed (in primary zone Z_1 and the secondary zone Z_2).

Because the plasticity is mainly transformed in heat, the energy balance in Z_1 is

$$\rho C_p \frac{\partial T(x,t)}{\partial t} = \beta \omega'_{plast} \tag{5}$$

where β is the Taylor–Quinney coefficient defined in 0,9 [26] and ω'_{plast} in W/m^3 is the power generated by the plasticity work, and so

$$\rho C_p \frac{\partial T(x,t)}{\partial t} = \beta(\sigma : \dot{\varepsilon}_p) \tag{6}$$

where σ (Pa) is the stress in the primary shear plan, and $\dot{\varepsilon}_p$ (s^{-1}) is the strain rate in the same zone.

Concerning the secondary shear zone where the phenomena are mainly friction, the heat equation becomes

$$\rho C_p \frac{\partial T(x,t)}{\partial t} = \omega'_{friction} = \eta \tau_f V_{friction} \tag{7}$$

where $\omega'_{friction}$ is the power generated by the friction (W/m^3), τ_f is the shear strain (s^{-1}), $V_{friction}$ is the sliding velocity (m/s), and η is the proportion of energy dissipated in heat.

However, and according to the micrographies, it seems difficult to define accurately the stress and the strain which occurred in both zones. The solution proposed in this study is to separate the energy contribution of each zone. For example, Ma et al. [27] define for stainless steel, the ratio between W_{Z2} and W_{ext} is 0.7. The other possibility is to set this ratio (R_w) in using partially Oxley's model

$$R_w = \frac{W_{ext}}{W_{Z1}} = \frac{F_c V_c}{F_s V_s} \tag{8}$$

where

$$F_s = F_c \cos(\phi) - F_r \sin \phi \tag{9}$$

and

$$V_s = \frac{V_c \cos(\alpha)}{\cos(\phi - \alpha)} \tag{10}$$

where F_s is the primary shear force in N, ϕ is the shear angle (rad), α is the rake angle (rad), and V_s is the primary shear velocity (m/s).

For this alloy, the ratio is constant and always equal to 0.7. Consequently

$$\rho C_p \int_{V_{Z1}} \frac{\partial \bar{T}_1}{\partial t} = \int_{V_{Z1}} \beta \omega'_{plast} dV = \int_{V_{Z1}} \omega'_{heat} dV \tag{11}$$
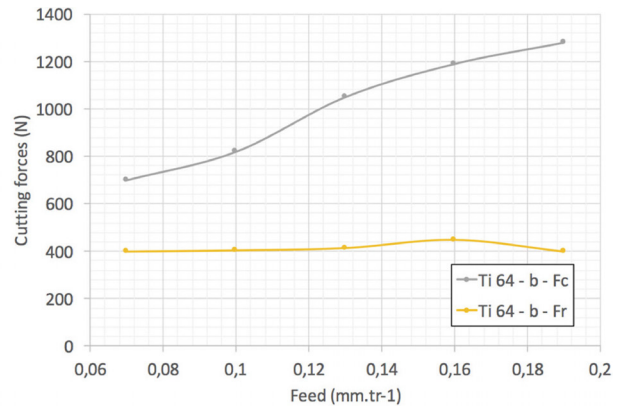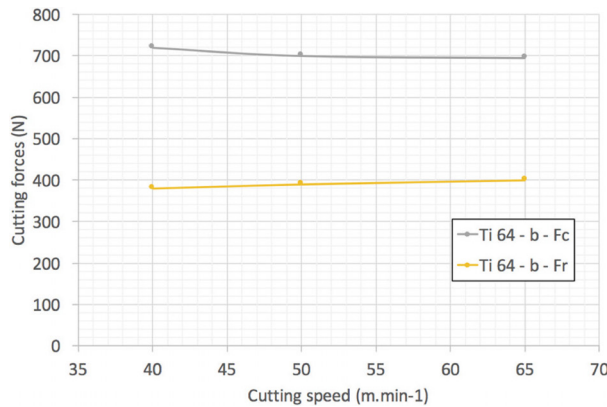

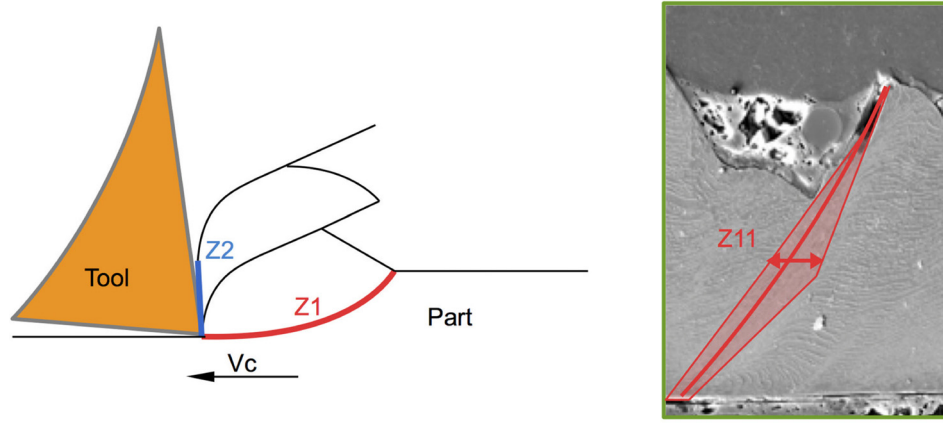**Fig. 8** Cutting forces for all cutting conditions

Fig. 9 Chip formation and model used for cutting temperatures

where V_{Z1} is the volume of sheared material in the primary zone in (m³). This volume is also measured according to metallographics analysis, $\bar{T}$ is the temperature increase

Consequently

$$V_{z1}\rho C_p \frac{\partial \bar{T}_1}{\partial t} = \frac{W'_{\text{heat1}}}{\beta} = R_w W'_{\text{ext}} \quad (12)$$

For the second shear zone, the method applied is the same

$$V_{z2}\rho C_p \frac{\partial \bar{T}_2}{\partial t} = \frac{W'_{\text{heat2}}}{\beta} = \left(1 - \frac{1}{R_w}\right) W'_{\text{ext}} \quad (13)$$

For this study and because, the work concerns the chip formation, only the temperature in the primary bands will be considered. It is possible to define the temperatures in each shearing band as a function of cutting conditions. Each volume V_{Z1} is measured using the software IMAGEJ (Fig. 9). The specific heat C_p and the density ρ are kept constant, despite their relations with the temperatures.

First, temperatures evolution is never steady and evolves with the bands geometry (Fig. 10). By comparing some bands, it is possible to understand its evolution. The band $Z11$ compared to the band $Z12$ is shorter, but the volume sheared is the same. Consequently, the temperature increases in $Z12$. Indeed, the time required to form the band is longer and allows the heat generation. At the opposite, the lengths of $Z12$ and $Z15$ are the same but the volume sheared for $Z15$ is smaller. Consequently, the temperature increases drastically. The cutting speed is the same, the bands are generated on the same period but the very small volume increases the temperatures. Latest example between the bands $Z13$ and $Z17$: the volumes are similar but the length of $Z13$ is smaller. Consequently, the temperature in $Z17$ increases.

Table 2 Evolution of shear angle, cutting temperatures, and standard deviation for all cutting conditions

V_c (m/min)	t_u (mm)	ϕ (rad)	DT (K)	Standard deviation DT (K)
40	0.07	33	1452	437
50	0.07	32	1698	462
65	0.07	30	2025	56
65	0.1	22	2033	289
65	0.13	28	1957	169
65	0.16	30	1862	472
65	0.19	20	1866	486

The almost instantaneous evolution leads to have a constant temperature inside the chip as observed by Wagner et al. [8]. The method elaborated in this paper defines only the increase of temperature generated in the primary bands during its formation and explain their high levels. These temperatures corroborate with the high level of temperature balance observed in other papers [16]. These phenomena are not observable on the cutting forces where the variations are not observable. Moreover, temperatures evolution between each band defined with the model can explain the high instability of chip flow as observed by Barelli et al. [28]. This high instability in the primary zone can also induce an instability in the secondary zone (not studied in this paper) in temperature or in pressure (variation of contact length of chip on the rake face) and generate a thermal fatigue.

This model can be utilized to compare the effect of the cutting conditions on the cutting temperatures (Table 2). The temperatures noted in the table are the average temperatures of five bands. As demonstrated by Wagner et al. [8] and Hoyne et al. [29], the increase of cutting speed generates higher temperature, explained
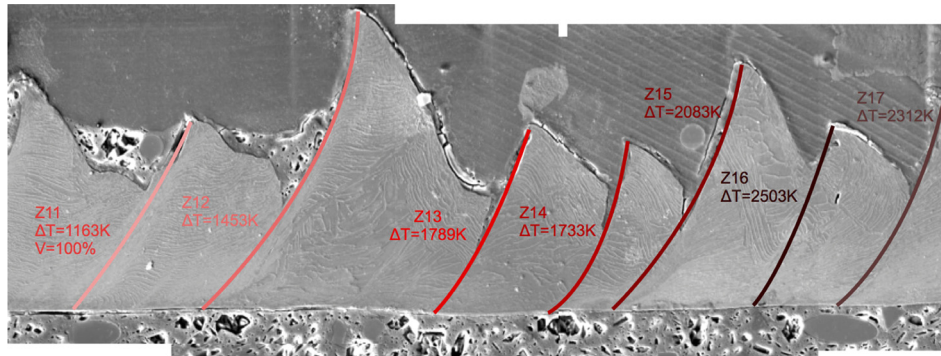

Fig. 10 Evolution of temperature for each shearing band when $V_c = 65$ m/min and $t_u = 0$, 16 mm

by the highest strain rate and by the reduction of the time to generate the primary shear band. Contrary to the effect of the feed which decreases the temperature, this lower temperature is due to the highest volume of sheared material and the increase in the length of the bands. Concerning the standard deviation, its evolution can be explained through the observation of chip morphology evolution according to cutting conditions, as exposed in Sec. 4.2.

Despite the high temperatures, higher to the β transus temperature, it seems very difficult to work on the effect of the temperature on the microstructure. Indeed, the microstructure of the chip analyzed is modified by the cooling kinetic of alloy and limits the analysis.

4.2 Chip Formation. Section 5 exposes the effect of the cutting speed on the chip formation. As defined previously, the chip formation is not constant. Consequently, different chip morphologies are shown for the same conditions. First, when $V_c = 50$ m/min, some wider sheared bands are generated. For the highest cutting speed, the chip formation does not evolve (Table 3).

Table 4 shows the effect of feed on the chip formation. When t_u increases, some shear bands are generated in the colonies which are not favorably oriented. Indeed, the increase in the feed generates higher shear forces and can induce the creation of shear bands. Moreover, the size of the crack between the chip teeth is also greater. When the feed increases, the higher shear forces

generate a constant chip. Indeed, the frequency between shears becomes constant. The chip generated when $t_u = 0.19$ mm is the same as that with the previous feed. Moreover, this analysis shows that the relation between the shear angle and feed is not direct. Contrary to the Merchant model, it is not possible to define the shear angle according to feed and chip thickness. This phenomenon is due to the microstructure's heterogeneity.

5 Chip Formation Discussion

In this section, the chip formation is discussed. As seen previously, the chip formation is a function of the cutting conditions and the orientation of the structure on which the adiabatic shear band will be generated. This section is dedicated to defining the different possibilities for adiabatic shear bands' formation in the primary zone. Different studies show that the chip formation is mostly a function of the phenomena generated in this zone.

The state of the art highlights different types of chips [1]. As seen previously, two types of chips have been observed: continuous chips and the segmented chips. The continuous chips, whose thickness is stable, are often generated when the stresses in the workpiece material are too weak to achieve segmentation. The segmented chips are characterized by saw teeth and a variable thickness. However, and contrary to the $\alpha + \beta$ structure, different types of chips can be generated in the same cutting conditions.

Table 3 Chip formation Ti64 β structure when $t_u = 0$, 1 mm and $V_c = 40$ m/min in the first line, $V_c = 50$ m/min in the second line, and $V_c = 65$ m/min in the last line
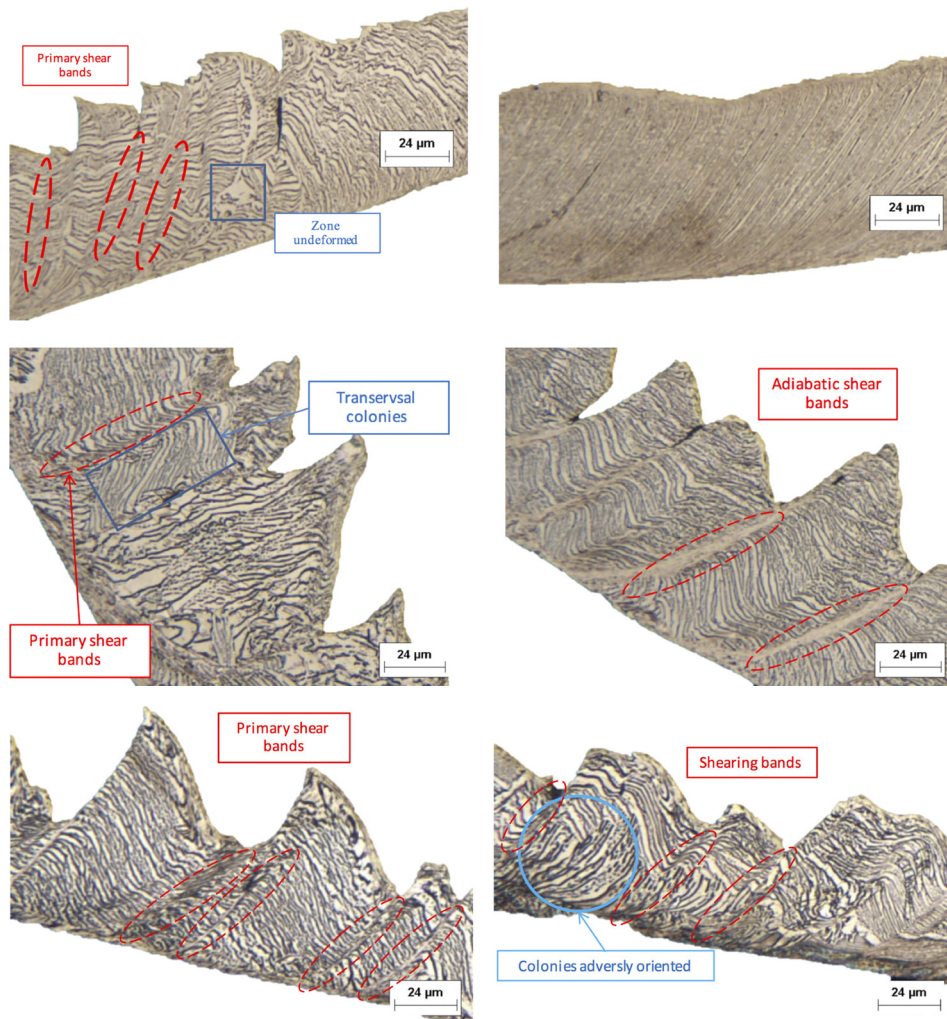
Moreover, the phenomena which govern the chip formation are somewhat different.

It is possible to predict the chip formation by analyzing the relationship between the microstructure and the shear direction. The analysis of the alloy microstructure indicates five possibilities where shear bands can be generated: a single colony (a), two colonies with a strong misorientation (b), two colonies with poor misorientation (c), the old β grain (d), and the old structure (e) (Fig. 11). In this study, the old structure will be the bimodal structure where the transformation in the β structure is not complete. For all these possibilities, the shear band may be generated in different directions: normal to the lamellar colonies (red arrow) or collinear to the lamellae (green arrow).

For the first possibility (a), different observations show that the primary shear can progress in line with the colony orientation. If the shearing direction is collinear to the colony (green arrow), the

shearing is continuous. This chip formation is explained by the ease to spread shearing inside the material. When the shearing direction is transverse to the colonies, some shear bands occur. They are caused by the strain gradient between the β lamellae which increases near the boundaries. The stress needed to shear boundaries is also greater than the shear required to deform the α lamellae. Consequently, when the primary shear band formation begins, stress occurs inside the material and the shear band propagates in the easiest way: the α lamellae. When the cutting speed increases, the thermal energy becomes greater and enables the formation of shear bands. The tests demonstrate that the primary shear bands' thickness increases with the cutting speed. This is explained by the higher thermal energy dissipated.

Concerning the second configuration (b), whatever the cutting speed, when the shear is generated between two colonies a crack is formed. This is explained by dislocation accumulation at the

Table 4 Chip formation Ti64 β structure when $V_c = 65$ m/min and $t_u = 0$, 1 mm in the first line, $t_u = 0$, 13 mm in the second line, $t_u = 0$, 16 mm in the third line, and $t_u = 0$, 19 mm in the last line
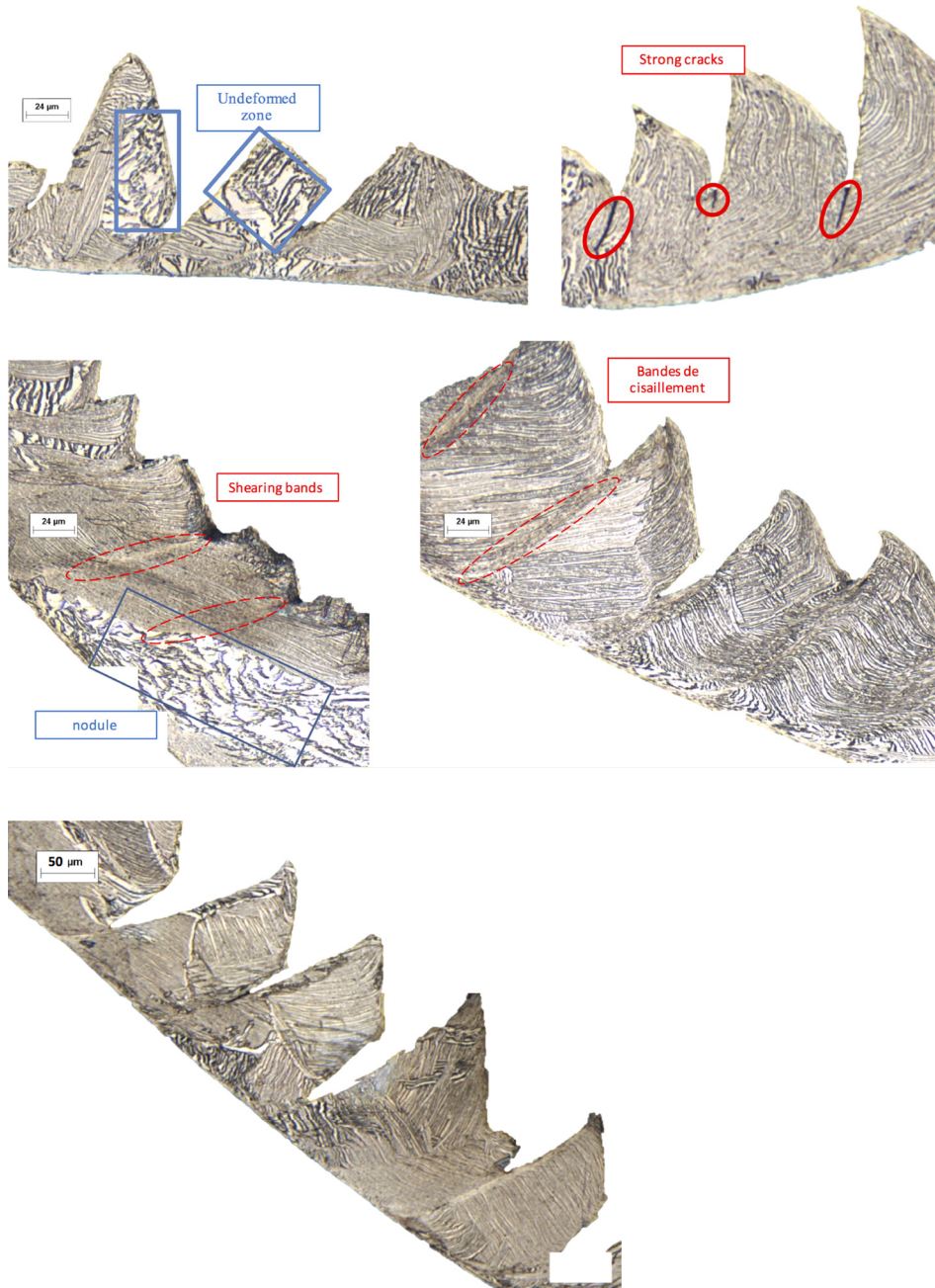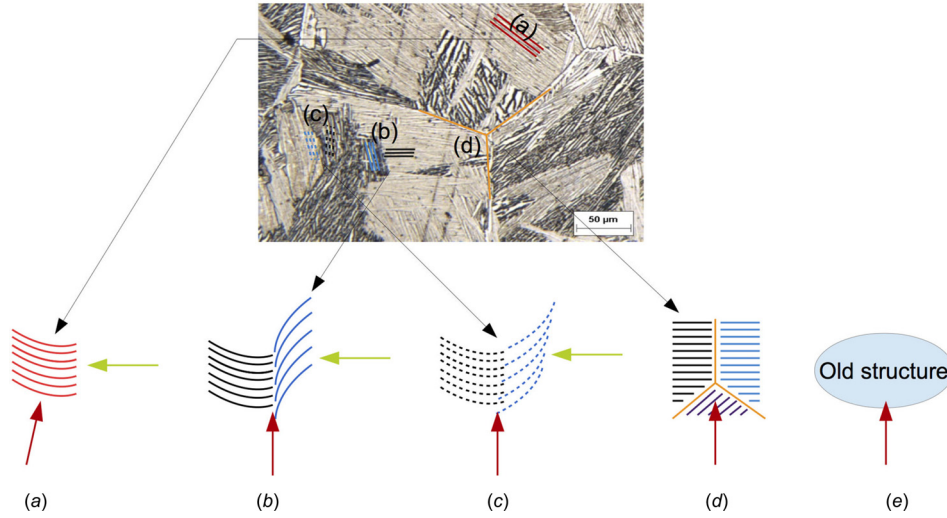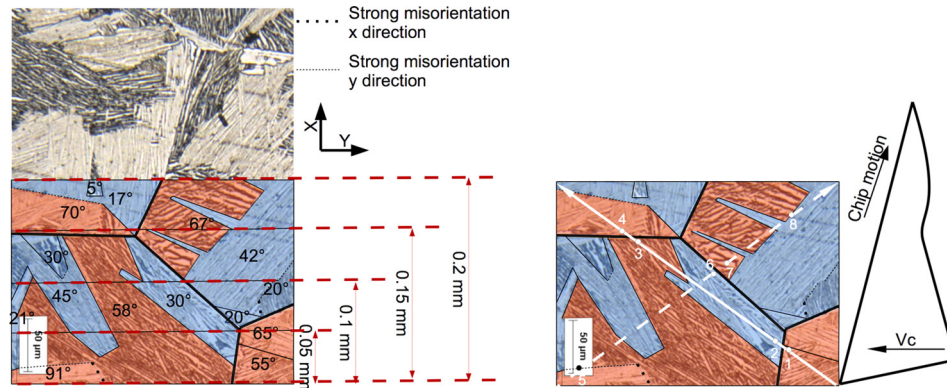
Fig. 11 Chip formation Ti64 β structure

Fig. 12 Effect of feed on chip formation

interface, leading to high plastic strains and stress stacking. Thus, a crack is initiated. When the cutting speed increases, cracks are larger. However, the crack height seems mostly to be influenced by the colonies' orientation.

Contrary to the aforementioned possibility, when the shear band propagates between two colonies where the lamellae are col-inear, a shear band is generated (*c*). However, the tests show that the shear bands are always thinner in this configuration compared to the other configuration.

Some old β grains may be present in the structure and as with the old structure, shear bands cannot propagate. Indeed, the shear-ing seems to be facilitated through the lamellae, and it is stopped in the other structures.

The last point is the effect of the feed. When the feed increases, the shear forces and the deformation rise. But, for this alloy, this increase leads to a different material being machined, since the probability of getting many different colonies in the thickness grows. Figure 12 shows the structure of titanium with the β struc-ture, the feeds used for the tests, and the colony orientation based

on two directions (*X* and *Y*). Two types of orientation are indi-cated: in light color (blue), the colonies whose lamellae angles are higher than 45 deg from the *X* direction; in dark color (orange), the colonies whose lamellae angles are lower than 45 deg. All the directions and the surface have been identified with IMAGEJ soft-ware. This short analysis can be compared to the probability of shearing a colony with an inclination. Based on this figure, it is now possible to define the part of the lamellae inclination when the shear band propagates in *X* positive and negative directions and for different feeds. The part of lamellae is the ratio between the whole section (on the picture) for different feeds and the orange section. As seen in Fig. 12, the structure is totally different when the feed increases or when the feed starts from an other point. For example, when $t_u = 0.05\,\mathrm{mm \cdot tr^{-1}}$, the proportion of lamellae inclined with an angle higher than 45 deg is 81%. This proportion decreases to 58% when the feed increases to $t_u = 0.1\,\mathrm{mm \cdot tr^{-1}}$ (Table 5).

Different patterns can be considered depending on the cutting speed and shear band direction. For this demonstration, the feed is fixed to $t_u = 0.2\,\mathrm{mm \cdot tr^{-1}}$. Two cutting directions are used. The first is a motion of the tool to the left. Consequently, the primary shear band generated is the continuous arrow. The shear angle is approxi-mately 35 deg. Because the tool moves to the left, the chip slides on the rake face and follows the chip motion. The same demonstration will be done with a tool which moved to the right. For this case, the primary shear bands generated are depicted by the dotted arrow.

Concerning the first case, the chip formation begins in a trans-verse colony. An adiabatic shear band is then generated. It is stopped between points 1 and 2 (on the left figure) due to the old

Table 5 Effect of feed on the lamellae inclination proportion

XC (mm)	Positive *X* direction (%)	Negative *X* direction (%)
0.05	81	53
0.1	58	42
0.15	49	39
0.2	50	50

β grain boundary. Between 2 and 3, the previous observations suggest that there is no shearing. Indeed, the shear band is stopped, and it cannot reappear because a second old grain boundary occurs between 3 and 4. Consequently, the chip formed can be assimilated to a continuous chip. For the second case, the structures encountered during the chip formation are different. The chip formation also begins by a transverse colony. Thus, adiabatic shear bands are generated. At point 5, there is a boundary where a strong misorientation between lamellae occurs. The foregoing observations serve to define two scenarios. The first is transmission of the adiabatic shear band through the boundary, and the second is the formation of a crack. The scenario is dependent on the cutting speed. Indeed, for a high cutting speed, a large adiabatic band is created, suggesting that the adiabatic shear bands continue through the limit. If the cutting speed is low, the adiabatic shear band is thin and a crack can be initiated. Between points 5 and 6, the adiabatic shear band is generated because the lamellae are transverse to the adiabatic shear formation. The shearing is then stopped between points 6 and 7. Contrary to the previous case, a crack can be generated. Indeed, near point 8, the different colonies are misoriented. A large crack can be formed and shearing can occur due to the previous shear bands formation (configuration 4).

6 Conclusion

The paper presents the study of chip formation in a specific structure of Ti64 titanium alloy. After outlining the experimental setup, the material is exposed. The second section of the article introduces the analysis of the chip formation. Contrary to the classical or bimodal structure, it is not a homogeneous one. Some zones are observed where the structure is different. This heterogeneity generates a specific chip formation and above all a chip formation that progresses in the chip thickness. The chip formation study shows that the primary shear bands formation is also a function of the cutting conditions but especially a function of the relation between the primary shear bands direction and the slate direction. For example, for a single colony, if the primary shear band direction is colinear to this colony, a continuous chip is generated. However, if the shear band direction is transverse to the colony, a shear band is created, and the chip is a saw-tooth chip. To understand and explain the formation of chips, an analysis of all opportunities (the relationship between the structure and direction of the shear band) was performed. This analysis predicts chip formation dependent upon the structure encountered by the shear band.

Acknowledgment

References

[1] Komanduri, R., and Von Turkovich, B. F., 1981, "New Observations on the Mechanism of Chip Formation When Machining Titanium Alloys," Wear, **69**(2), pp. 179–188.

[2] Vyas, A., and Shaw, M. C., 1999, "Mechanics of Saw-Tooth Chip Formation in Metal Cutting," ASME J. Manuf. Sci. Eng., **121**(2), pp. 163–172.

[3] Barry, J., Byrne, G., and Lennon, D., 2001, "Observations on Chip Formation and Acoustic Emission in Machining Ti–6Al–4V Alloy," Int. J. Mach. Tools Manuf., **41**(7), pp. 1055–1070.

[4] Nouari, M., and Makich, H., 2013, "Experimental Investigation on the Effect of the Material Microstructure on Tool Wear When Machining Hard Titanium Alloys: Ti–6Al–4V and Ti-555," Int. J. Refract. Met. Hard Mater., **41**, pp. 259–269.

[5] Wagner, V., and Duc, E., 2014, "Study of Ti-1023 Milling With Toroidal Tool," Int. J. Adv. Manuf. Technol., **75**(9–12), pp. 1473–1491.

[6] Braham-Bouchnak, T., Germain, G., Morel, A., and Furet, B., 2015, "Influence of High-Pressure Coolant Assistance on the Machinability of the Titanium Alloy Ti555–3," Mach. Sci. Technol., **19**(1), pp. 134–151.

[7] Arrazola, P.-J., Garay, A., Iriarte, L.-M., Armendia, M., Marya, S., and Maitre, F. L., 2009, "Machinability of Titanium Alloys (Ti6Al4V and Ti555. 3)," J. Mater. Process. Technol., **209**(5), pp. 2223–2230.

[8] Wagner, V., Baili, M., and Dessein, G., 2015, "The Relationship Between the Cutting Speed, Tool Wear, and Chip Formation During Ti-5553 Dry Cutting," Int. J. Adv. Manuf. Technol., **76**(5–8), pp. 893–912.

[9] Yessine, A., Guénaël, G., Amine, A., and Benoit, F., 2013, "Degradation Modes and Tool Wear Mechanisms in Finish and Rough Machining of Ti17 Titanium Alloy Under High-Pressure Water Jet Assistance," Wear, **305**(1–2), pp. 228–237.

[10] Shaw, M. C., and Vyas, A., 1998, "The Mechanism of Chip Formation With Hard Turning Steel," CIRP Ann. Manuf. Technol., **47**(1), pp. 77–82.

[11] Recht, R. F., 1964, "Catastrophic Thermoplastic Shear," ASME J. Appl. Mech., **31**(2), pp. 186–193.

[12] Viktor, P. A., 2004, "Tribology of Metal Cutting," Mechanical Tribology, Elsevier, Amsterdam, The Netherlands, pp. 307–346.

[13] Manyindo, B. M., and Oxley, P. L. B., 1986, "Modelling the Catastrophic Shear Type of Chip When Machining Stainless Steel," Proc. Inst. Mech. Eng., Part C, **200**(5), pp. 349–358.

[14] Guosheng, S., and Zhanqiang, L., 2013, "Analytical and Experimental Study on Formation of Concentrated Shear Band of Saw Tooth Chip in High-Speed Machining," Int. J. Adv. Manuf. Technol., **65**(9–12), pp. 1735–1740.

[15] Pottier, T., Germain, G., Calamaz, M., Morel, A., and Coupard, D., 2014, "Sub-Millimeter Measurement of Finite Strains at Cutting Tool Tip Vicinity," Exp. Mech., **54**(6), pp. 1031–1042.

[16] Harzallah, M., Pottier, T., Senatore, J., Mousseigne, M., Germain, G., and Landon, L., 2017, "Experimental Investigations of Ti-6al-4v Chip Generation and Thermo-Mechanical Couplings in Orthogonal Cutting," Int. J. Mech. Sci., **134**, pp. 189–202.

[17] Sutter, G., and List, G., 2013, "Very High Speed Cutting of Ti–6Al–4V Titanium Alloy–Change in Morphology and Mechanism of Chip Formation," Int. J. Mach. Tools Manuf., **66**, pp. 37–43.

[18] Calamaz, M., Coupard, D., and Girot, F., 2008, "A New Material Model for 2d Numerical Simulation of Serrated Chip Formation When Machining Titanium Alloy Ti–6Al–4V," Int. J. Mach. Tools Manuf., **48**(3–4), pp. 275–288.

[19] Zhang, X., Shivpuri, R., and Srivastava, A. K., 2016, "Chip Fracture Behavior in the High Speed Machining of Titanium Alloys," ASME J. Manuf. Sci. Eng., **138**(8), p. 081001.

[20] Nguyen, T., Kwon, P., Kang, D., and Bieler, T. R., 2016, "The Origin of Flank Wear in Turning Ti–6Al–4V," ASME J. Manuf. Sci. Eng., **138**(12), p. 121013.

[21] Philippe, C., Besse, M., and Thierry, G., 2012, "In Situ Tem Study of Dislocation Slip in a Metastable β Titanium Alloy," Scr. Mater., **66**(6), pp. 371–373.

[22] Lütjering, G., 1998, "Influence of Processing on Microstructure and Mechanical Properties of ($\alpha+\beta$) Titanium Alloys," Mater. Sci. Eng.: A, **243**(1), pp. 32–45.

[23] Lütjering, G., and Williams, J. C., 2003, Titanium, Vol. 2, Springer, New York.

[24] AFNOR, 1994, "Tool-Material-Pair. Domaine De Fonctionnement Des Outils Coupants, AFNOR, Saint-Denis, France, Standard No e 66-520-6.

[25] Joshi, S., Tewari, A., and Joshi, S., 2013, "Influence of Preheating on Chip Segmentation and Microstructure in Orthogonal Machining of Ti6al4v," ASME J. Manuf. Sci. Eng., **135**(6), p. 061017.

[26] Cotterell, M., Ares, E., Yanes, J., López, F., Hernandez, P., and Peláez, G., 2013, "Temperature and Strain Measurement During Chip Formation in Orthogonal Cutting Conditions Applied to Ti–6Al–4V," Procedia Eng., **63**, pp. 922–930.

[27] Ma, J., Ge, X., Chang, S. I., and Lei, S., 2014, "Assessment of Cutting Energy Consumption and Energy Efficiency in Machining of 4140 Steel," Int. J. Adv. Manuf. Technol., **74**(9–12), pp. 1701–1708.

[28] Barelli, F., Wagner, V., Laheurte, R., Dessein, G., Darnis, P., Cahuc, O., and Mousseigne, M., 2016, "Orthogonal Cutting of TA6V Alloys With Chamfered Tools: Analysis of Tool–Chip Contact Lengths," Proc. Inst. Mech. Eng., Part B, **231**(13), pp. 2384–2395.

[29] Hoyne, A. C., Nath, C., and Kapoor, S. G., 2015, "On Cutting Temperature Measurement During Titanium Machining With an Atomization-Based Cutting Fluid Spray System," ASME J. Manuf. Sci. Eng., **137**(2), p. 024502.